Assessing Spatial-Temporal Characteristics of Land Desertification from 1990–2020 in the Heihe River Basin Using Landsat Series Imagery

Jie Liao , Xianzhong Yang , Qiyan Ye , Kaiming Wan , Jixing Sheng , Shengyin Zhang , Xiang Song *

Posted Date: 4 June 2024

doi: 10.20944/preprints202406.0179.v1

Keywords: Land Desertification, Spatial-temporal Pattern, Driving factors, the Heihe River, Landsat Imagery

Article

Assessing Spatial-Temporal Characteristics of Land Desertification from 1990-2020 in the Heihe River Basin Using Landsat Series Imagery

Liao Jie [1,†], Yang Xianzhong [2,†], Ye Qiyan [3], Wan Kaiming [3], Sheng Jixing [3], Zhang Shengyin [1] and Song Xiang [1,*]

[1] Northwest Institute of Eco-Environment and Resources, Chinese Academy of Sciences, No. 320 West Donggang Road, Lanzhou, Gansu Province, 730000, China
[2] Gansu Academy of Agri-Engineering Technology, No.18 Gaoxinyannan Road, Chengguan District, Lanzhou, Gansu Province, 730000, China
[3] Zhangye Heihe Wetland National Nature Reserve Administration, No.13 Xianfu South Street, Ganzhou District, Zhangye City, Gansu Province, 734000, China
* Correspondence: songxiang@lzb.ac.cn. Tel.: +86-931-496-7553
† These authors contributed equally to this work.

Abstract: Monitoring the status and dynamics of desertification is one of the most important parts of combating desertification. In this study, 30m high-resolution information on land desertification and restoration in the HRB was extracted from the land cover database. The results indicate that land desertification coexists with land restoration in the HRB. At different periods, the area of land restoration is much larger than the area of land desertification in the HRB, and the HRB has been in a process of land restoration. Upstream of the HRB, there is a continuing trend of increasing land desertification associated with overgrazing in a context where climate change favors desertification reversal. In the middle and lower reaches, although both climate variability and human activities favor land desertification, the process of land desertification in the middle and lower reaches is still being reversed and land restoration dominates. The implementation of the Eco-Environmental Protection Project and desertification control measures, especially the EWDP, is contributing to the reversal of desertification in the middle and lower reaches of the HRB. However, the EWDP has indirectly led to the lowering of the water table in the middle reaches, resulting in local vegetation degradation. Therefore, there is therefore an urgent need to transform the economic structure of the middle reaches to cope with water scarcity and land desertification.

Keywords: land desertification; spatial-temporal pattern; driving factors; the Heihe River; Landsat imagery

1. Introduction

Land desertification, known as the "cancer of the earth", is one of the top ten major environmental problems in the world (Wu et al. 2019) and a challenging issue in global ecological governance (Yan et al. 2015). UNCCD (1999) defines land desertification as a form of land degradation in dryland, which includes arid, semi-arid, and dry subhumid areas, driven by several interrelated factors and triggered by the combination of climate change with irrationality of human activities. The combination of global warming, rapid economic development, urban expansion and population growth (Tavares et al. 2015; Xu et al. 2016; Zhao et al. 2024) has increased the extent and intensity of desertification in some dryland areas over the past numerous decades (Burrell et al. 2018; Gichenje and Godinho 2018). Desertification causes serious environmental issues and leads to some significant negative impacts on socioeconomic development, such as food shortages, poverty, and health problems (Huang et al. 2016; Koutroulis 2019; Lee et al. 2016; Ma et al. 2021), which have become one of the important factors hindering sustainable development in drylands (Guo et al. 2022; Li et al. 2016). Considering the potential negative impacts of desertification on the environment,

 doi:10.20944/preprints202406.0179.v1

socioeconomic development, desertification prevention and control was included as one of the SDGs in the 2030 Agenda for Sustainable Development, which aims to "*protect, restore and promote sustainable use of terrestrial ecosystems, sustainably manage forests, combat desertification, and halt and reverse land degradation and halt biodiversity loss*" (Nations 2016). To achieve the goal of Land Degradation Neutrality by 2030, combating desertification plays a critical role in conserving biodiversity, mitigating human-induced global warming, and eradicating global poverty.

China is one of the countries most affected by desertification. According to the Sixth Survey of Desertification in China, as of 2019, the area of desertified land nationwide reaches 2,537,000km^2, accounting for nearly 27% of total land area, of which 65.6% is aeolian desertified land(ADL), and more than 16% of ADL still had a tendency to desertify (Zan et al. 2023). In China, the most seriously areas of desertification are mainly concentrated in the northwestern and northeastern regions, which not only seriously jeopardize the local ecological environment but also are the main source area of spring sandstorms in China (Zhang and Huisingh 2018). The Heihe River Basin (HRB) in the inland semi-arid and arid zones of northwest China is a typical ecologically fragile area because of desertification. In the HRB, water scarcity is the single most limiting factor for ecological restoration and socioeconomic development. Against the backdrop of climate change, although the climate trends to warm and humid in the northwestern China, increased precipitation is not sufficient to offset increased evaporation from higher temperature duo to a small precipitation base (Shi et al. 2003). Coupled with the surge in water demand from oasis agriculture and urbanization in the middle reaches of the HRB (Zhang et al. 2015), the sensitivity and vulnerability of ecosystems are further exacerbated, which has made the downstream of the HRB one of the major sources of sandstorms (Wang and Cheng 1998). To resolve water resource conflicts in different regions of the HRB, the Chinese government has implemented the Ecological Water Diversion Project (EWDP) to ensure that the ecological water demand downstream of the HRB is met, thereby mitigating and restoring ecological desertification in the downstream oases since 2000. However, it is still unclear whether the EWDP contributes to the reversal of desertification and how climate change and human activities influence the desertification process. Therefore, studying the spatio-temporal characteristics of desertification and its driving mechanisms is of great importance for the adaptation and formulation of subsequent desertification control and ecological restoration measures in the HRB.

Accurate monitoring of the status and dynamics of desertification is one of the most important parts of combating desertification. However, the traditional methods of desertification monitoring have the disadvantages of long consumption, labor-intensive and costly, inefficient, small spatial scales, and so on (Christian and Dhinwa 2018). With the rapid development of remote sensing and Geographic Information System technology, satellite remote sensing provides an economical, efficient, effective, and objective approach to assess land desertification over long periods from regional to global scales (Li et al. 2023; Song et al. 2020a; Song et al. 2015; Zhao et al. 2024). Methods of applying remote sensing and GIS to monitor land desertification can be broadly categorized into three groups: 1)the use of vegetation indices to estimate desertification processes (such as NDVI, MSAVI, EVI, and NPP, etc.) (Mariano et al. 2018; Shen et al. 2018; Wessels et al. 2012), and in some cases land surface and climate parameters such as Albedo, TVDI, TGSI, LST, Precipitation, Temperature, Evapotranspiration, etc., are often used for more accurate results (Duan et al. 2019; Lamchin et al. 2016; Liu et al. 2018); 2) Extraction of desertification information by visual interpretation or automatic classification using Landsat imagery (Li et al. 2023; Meng et al. 2021; Zhang et al. 2018); 3) using the feature space models for classification, such as Albedo-NDVI model (Wei et al. 2020) and point-point model (Guo et al. 2020). However, the use of method 1 to monitor desertification relies on data with coarse spatial resolution (e.g., 8 km or 1 km) and can provide macro distribution and general trend with high temporal resolution, but details of desertification characteristics are not available. Methods 2 and 3 use data sources with high spatial resolution (e.g., Landsat series data with 30m resolution), but the monitoring results are overly dependent on the time of image acquisition and the classification method chosen, resulting in large differences in the interpretation results of images at different times, and the monitoring results do not truly reflect the characteristics and trends of desertification.

 doi:10.20944/preprints202406.0179.v1

Considering the above issues, this manuscript aimed to use object-oriented classification methods to assess desertification dynamics from 1990 to 2020 in the HRB based on Landsat imagery acquired from the GEE. A 30m resolution land cover dataset for 1990, 2000, 2010, and 2020 was established, and spatial analysis methods provided by GIS were used to analyze the changes in land cover types in 1990, 2000, 2010, and 2020 to obtain the characteristics of desertification in the HRB over the past 30 years. Finally, the dominant driving factors of the desertification and restoration processes were examined and discussed.

2. Materials and Methods

2.1. Study Area

The Heihe River is the second-largest inland river in China, originating from Lenglongling in the Qilian Mountains, flowing through Qinghai Province, Gansu Province, Inner Mongolia Autonomous Region, and finally flowing into the terminal lake Juyan Sea, with a total length of 821 km and a drainage area of 271,000 km^2, of which the area within the territory of China is about 87.6% and the rest is located in the territory of Mongolia (Figure 1). The Heihe River Basin is characterized by significant zonal differentiation, with a globally unique glacier-frozen soils-river-oasis-desert multidimensional natural landscape zone sequentially distributed with altitude. Due to the surrounding mountains and the distance from the sea, the HRB has a typical temperate continental climate with characteristics of low precipitation and higher evaporation. Depending on altitude, the temperature, precipitation, and evaporation in the HRB vary greatly on spatial and temporal scales. From south to north, as the altitude decreases, the annual mean temperature increases from 2 to 10 °C, precipitation decreases from 500 to less than 50 mm, and evaporation increases from 700 to more than 3500 mm. As of the end of 2014, the total population within China in the HBR was 2.52 million, with a population density of 10.5 people per km^2, of which 56.9% was agricultural. The population of the Heihe River Basin is concentrated in the middle reaches of the basin, accounting for 95.3% of the total population. The HRB is backward in terms of economic development, with a GDP of only 115.1 billion yuan in 2014 (Song et al. 2020).

 doi:10.20944/preprints202406.0179.v1

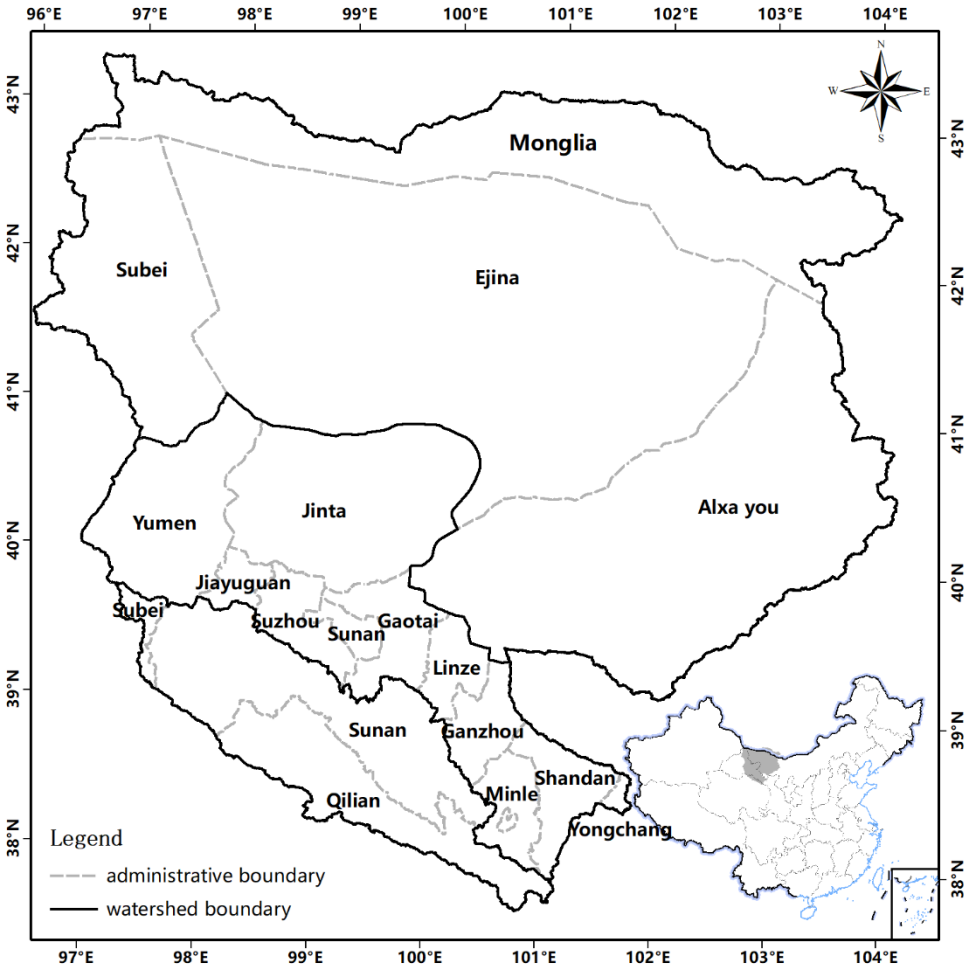

Figure 1. Location of the Heihe River Basin.

2.2. Data Sources

In this study, we mapped fine-resolution land cover distributions in 1990, 2000, 2010, and 2020 in the HRB by using an object-oriented classification method. The Landsat Collection 2 Surface Reflectance Tier 1 images (including TM, ETM+, and OLI) derived from the Google Earth Engine (GEE) in the study area were used to establish the land cover dataset for each period (Amani et al. 2020; Hird et al. 2017). All of these images were subjected to geometric and atmospheric correction, as well as cross-calibration between the different sensors (Dwyer et al. 2018; Wulder et al. 2016; Zhu et al. 2015). For each image, the CF mask, which is a cloud masking method, was used to remove clouds, cloud shadows, and snow pixels by using the data quality layer (Meng et al. 2021; Zhou et al. 2019; Zhu and Woodcock 2014). All the remaining pixels were considered to be good quality Landsat observations that could be used for land cover mapping. To reduce the influence of atmospheric noise and inter-annual phenological differences, the images from three different years were used to acquire high-quality observation composites for each period. (Chen et al. 2020). For example, the 2020 data were a synthesis of the good-quality growing-season pixels from the 2019, 2020, and 2021 images. Due to snow-covered and cloudy weather in areas above the snow line of the Qilian Mountain in the southern HRB, there are no good-quality observations in these areas. Considering that the unobserved area is small, and the land cover type is glacier and alpine desert, we believe it has little impact on this study. Finally, four phases of high-quality growing season Landsat image collections of the HRB with 30m spatial resolution, including bands of blue, green, and red, near infrared (NIR), short-wave infrared 1 (SWIR1), and short-wave infrared 2 (SWIR2), were generated based on GEE.

In addition, the auxiliary data used to assist in interpretation of the land cover data and the analysis of the driving factors behind desertification include the following: 1)Vegetation type map of

 doi:10.20944/preprints202406.0179.v1

China, with scale 1:1,000,000 (source: National Cryosphere Desert Data Center, http://www.ncdc.ac.cn); 2)DEM and slope data, with spatial resolution of 30 m (source: ASTER Global Digital Elevation Model V003, NASA Earth science data, https://www.earthdata.nasa.gov); 3)Meteorological data (Ejina Banner in Alax League of Inner Mongolia, Zhangye in the Hexi Corridor of Gansu Province and Qilian in the Qilian of Qinghai Province) including precipitation, annual mean temperature (source: the China Central Meteorological Bureau, http://cdc.cma.gov.cn); 4) Hydrological data(Yingluoxia (YLX), Zhengyixia (ZYX), and Langxinshan(LXS), source: the Heihe River Bureau); 5)Field survey data of land use/cover types in the HRB acquired in 2015.

2.3. Classification of Land Cover

In this study, the Automatic Object-Oriented Classification Based on Decision Tree was used to derive fine-resolution data for land cover. According to the China Land Cover Classification System, the National Land Use Remote Sensing Mapping Classification System (Zhang et al. 2014) and the characteristics of land cover in the HRB, we identified seven primary types of land cover in the HRB, including cropland, woodland, grassland, water bodies, wetland, artificial surface, and desert, which were divided into 16 secondary types (Table 1). Considering the small river area in the water area type, the low runoff, and the long breakup period in the middle and lower reaches of the HRB, we categorized the river type as bare soil to improve the accuracy of the classification.

Table 1. The land cover type classification system used in this study.

Primary types	Secondary types
Cropland	Paddy field, Non-paddy field
Woodland	Forest, Shrubs
Grassland	Meadow grassland, Typical grassland, Desert grassland
Water bodies	Lake, Reservoirs, and ponds
Wetland	Marsh
Artificial Land	Residential area, Industrial area, Traffic land, Mining land
Desert	Sandy, Barren

Based on the availability of reliable Landsat imagery, the study period was divided into three intervals (1990-2000, 2000-2010, and 2010-2020). The 2020 land cover dataset of the HRB is generated using Landsat OIL imagery, and the land cover datasets in the other periods were generated using Landsat TM imagery. In this study, the Automatic Object-Oriented Classification Based on Decision Tree was used to derive fine resolution data for land cover. First, we utilized the spectral difference segmentation and multiresolution segmentation algorithms provided by eCognition software (Definiens Imaging, Germany) to segment the images of 2020 into homogeneous polygons of different sizes according to the spectral difference and segmentation scale, which are named objects. Then, the segmented objects are classified according to texture, spatial, spectral, and shape features by using the decision tree method. In addition, to assist the classification and improve classification accuracy, the DVI, Fraction of Vegetation Cover (FVC), Top Grain Size Index(TGSI), Normalized Difference Water Index-Blue($NDWI_B$), and Normalized Difference Soil Index (NDSI) were calculated using the following equations:

$$
\begin{aligned}
NDVI &= (Nir - Red)/(Nir + Red) \\
FVC &= (NDVI - NDVI_{soil})/(NDVI_{veg} - NDVI_{soil}) \\
TGSI &= (Red - Blue)/(Red + Blue + Green) \\
NDWI_B &= (Blue - Nir)/(Blue + Nir) \\
NDSI &= (Swir1 - Nir)/(Swir1 + Nir)
\end{aligned}
$$

where Blue (TM=B1, OLI=B2), Green(TM=B2, OLI=B3), Red (TM=B3, OLI=B4), Nir(TM=B4, OLI=B5), and Swir1(TM=B5, OLI=B6) denote the reflectivity of the blue, green, red, near infrared, and short wave infrared 1 bands, respectively.

 doi:10.20944/preprints202406.0179.v1

Finally, 5% of the generated 10×10 km grid points, 468 in total, were randomly selected, and the land cover type of each point was manually interpreted using Google Earth ultra-high resolution imagery, which was used to assess the accuracy of land cover classification. If the accuracy of water area, grassland, woodland, cropland, and wetland types is less than 90%, these types met the accuracy requirement by increasing the decision tree classification index or adjusting the index threshold. Artificial surface, sand, and desert types are not easily confused with the above types, although they are confused with each other, so we use the method of visual interpretation combined with human-computer interaction to improve the classification accuracy.

After completing the 2020 land cover dataset, we utilized a knowledge-based object-oriented spectral vector change detection method to generate land cover datasets for 1990, 2000, and 2010. Taking 2010 as an example, the images of 2010, 2020, and 2020 land cover classification results were segmented by using eCognition software to generate objects. The reflectance of each band in different years of the object forms a spectral vector, and the similarity between the two vectors is calculated. The object whose similarity is less than the threshold value is the object that has been changed. According to the land cover type, 5% of the unchanged objects were randomly selected to calculate the average spectrum vector, and then the similarity between the vector of the changed object and the vector of each land cover type was calculated, and the changed objects were classified into the land cover type with the largest vector similarity pair. The details of classification and change detection method were described in Wu et al. (2014) and Song and Yan (2014).

2.4. Extraction of Land Desertification Information and Processing

Land desertification is the reduction or loss of biological or economic productivity and diversity of cropland, woodland, grassland, and pasture in a dryland region as a result of the utilization of the land or the impact of one or multiple factors (Ci 2000). Therefore, the process of land desertification can be characterized by changes in land cover. Based on the land cover change dataset, we classified woodland, meadow grassland and typical grassland as non-desertified land (NDL), and the areas that used to be NDL were transformed into desert grassland, sandy land, barren land as desertified land (DL). Using the spatial analysis module provided by Arcmap 10.8, the land cover datasets of the four periods were spatially overlapped to generate the land cover change datasets for the periods of 1990–2000, 2000–2010, and 2010–2020, respectively. Then, the distribution maps of desertification development and reversal are obtained by extracting the changed areas of DL and NDL land types as defined above in the HRB from 1990 to 2000, from 2000 to 2010, and from 2010 to 2020. By analyzing the status of land desertification in the HRB over time, we identified the trends of land desertification over a 30-year period and analyzed the driving factors of desertification development and reversal.

3. Results

3.1. Pattern of Land Cover Change from 1990 to 2020

In this study, to better understand the process, extent, and trend of land desertification or land restoration, not only NDL and DL but also other land cover types (including cropland, water bodies, artificial land, and wetland) were also counted. Table 3 presents the statistical data on the area of different land cover types in different parts of the HRB. Figure 2 illustrates the spatial distribution patterns of different land cover types.

 doi:10.20944/preprints202406.0179.v1

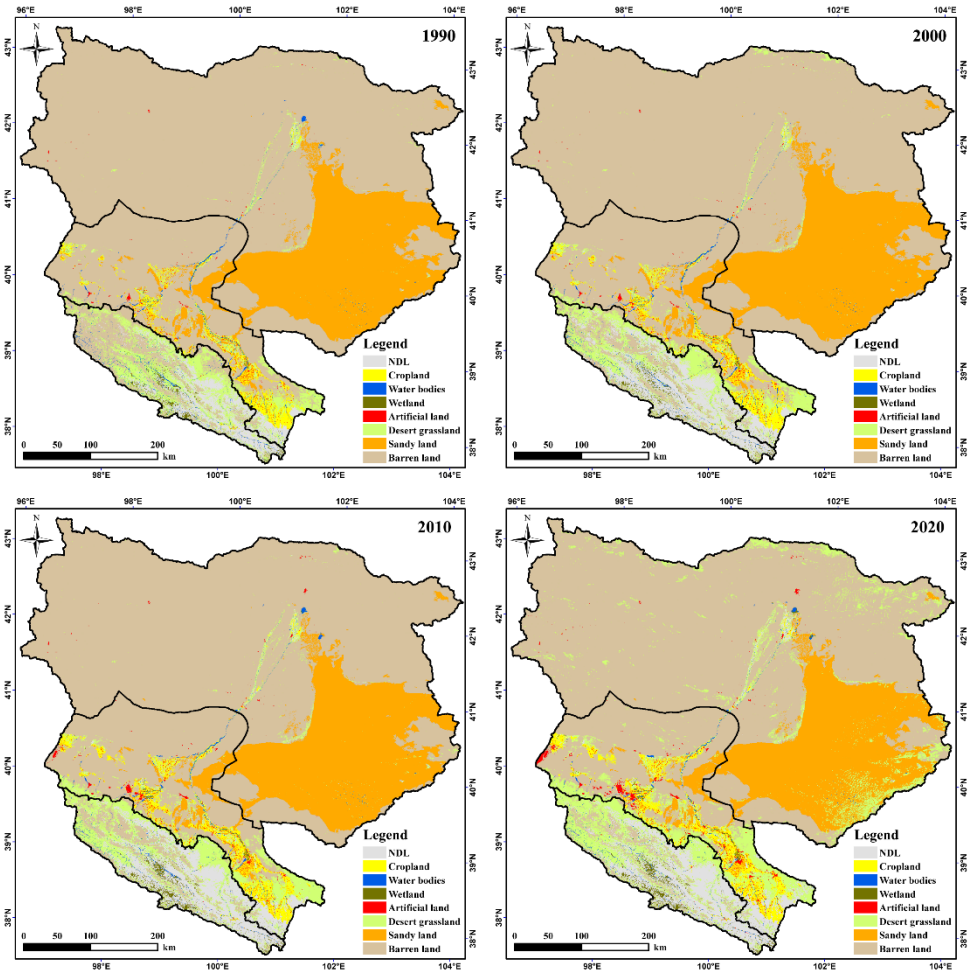

Figure 2. The pattern of different land types in the HRB in 1990, 2000, 2010, and 2020.

Table 2. Interpretation rules and reference index thresholds for land cover classification.

Land cover types	Rule and reference index threshold
Cropland	Compactness>2.5, visual interpretation
Woodland	NDVI>0.4, Red<0.06
Meadow steppe	NDVI>0.4, Red >0.06
Real steppe	0.4>NDVI>0.25, Red>0.1
Desert steppe	0.25>NDVI>0.1, Red>0.15
Water bodies	NDWI > 0
Artificial land	Visual interpretation
Wetland	NDVI> 0.4,Nir <0.24, Slope<10
Sand	NDVI<0.1, 2000>Brightness > 1000
Barren	NDVI<0.1, NDSI>0.09

Table 3. Areas of different land cover types in the HRB from 1990 to 2020 (km^2).

		Cropland	Water bodies	Artificial land	Wetland	NDL	Desert steppe	Sand	Barren
1990	Upstream	115.69	575.36	10.45	842.65	7231.48	8650.89		10226.86
	Midstream	5513.55	493.93	478.75	123.36	1466.92	3963.32	3474.57	39167.62
	Downstream	99.26	198.45	40.92	2.18	120.26	1046.25	45832.48	141342.70
	Total	5728.50	1267.75	530.12	968.19	8818.66	13660.47	49307.05	190737.18

 doi:10.20944/preprints202406.0179.v1

2000	Upstream	114.19	464.73	12.79	845.41	11789.02	8128.68		6298.55
	Midstream	6160.47	496.85	541.09	144.04	1644.88	4564.01	3413.22	37717.46
	Downstream	98.65	134.02	46.00	0.78	130.79	1447.49	45804.67	141020.12
	Total	6373.31	1095.60	599.87	990.23	13564.69	14140.18	49217.89	185036.13
2010	Upstream	103.24	450.00	18.77	1169.58	11809.60	8730.88		5371.30
	Midstream	6808.06	459.50	756.18	190.50	2252.93	6124.60	3261.41	34828.83
	Downstream	157.51	206.67	81.92	7.80	220.70	1318.31	45736.07	140953.53
	Total	7068.81	1116.17	856.87	1367.88	14283.23	16173.79	48997.48	181153.67
2020	Upstream	92.84	430.89	31.02	1215.02	12323.23	9504.85		4055.54
	Midstream	7540.87	426.20	1218.57	244.81	3131.72	9116.96	2974.12	30028.77
	Downstream	160.35	202.99	111.40	35.44	542.10	9015.42	43244.05	135370.76
	Total	7794.05	1060.08	1360.98	1495.27	15997.05	27637.23	46218.17	169455.08

In 1990, barren land was the most prevalent land cover type throughout the study period, accounting for 70.38% of the HRB. This land cove type is predominantly found in the west-central region of the HRB and is characterized by the Gobi, bare rock, bare land, and saline due to extremely dry and scarce rainfall. Because the Badain Jaran Desert, the third-largest desert in China, is located entirely downstream, sand is the second-largest land cover type, accounting for 18.19% of the HRB. Additionally, patches of quicksand were distributed adjacent to the edge of the midstream oasis. The vegetation type of the HRB is dominated by desert grassland, which accounts for 5.04% of the HRB and 63.32% of the area covered by vegetation. It is mainly distributed around oases in the middle and lower reaches, as well as in the pre-mountain floodplains in the upper reaches. Attributed to natural conditions, the proportion of NDL is relatively small, accounting for only 3.25% of the HRB. It is mainly found in the mountainous regions upstream, including coniferous forests, shrubs, alpine meadows, and alpine steppes, and there are also sporadic shrub forests and deciduous forests in the middle and lower reaches of the HRB along both sides of the river. Since the population of the HRB is concentrated in the midstream, the vast majority of cropland and artificial land is located here, which accounts for 2.11%, 0.20%, respectively. Water bodies and wetlands are predominantly located in the upstream of the HRB, accounting for 0.47%, 0.36%, respectively. Water bodies and wetlands are dominated by rivers and marshy meadows in the upstream and reservoirs, lakes, and riparian wetlands in the midstream and downstream.

With climate variability and rapid economic development, between 1990 and 2020, the coverage of cropland, artificial land, wetland, NDL, and desert steppe increased by 36.06%, 156.73%, 54.44%, 81.40%, and 102.32%, respectively, while the coverage of water bodies, sand, and barren decreased by 16.38%, 6.26%, and 11.16%, respectively. From the perspective of the different subregions of the HRB, the observed trends in the land cover types are also different. The NDL, sand, barren, wetland, and artificial land demonstrate a similar trend across the HRB, with the NDL, wetland, and artificial land exhibiting an increasing trend and the sand and barren exhibiting a decreasing trend. Although the area of cropland continues to increase, the upstream cropland shows a continuous decrease due to the implementation of ecological protection and restoration programs such as the “Grain for Green” project and the rapid development of urban construction. In contrast, the downstream cropland shows a decreasing and then increasing trend due to the changes in water resources. In this study, river floodplains are also classified as water bodies. It can be observed that the area of water bodies in the middle and upper reaches of the HRB continues to decrease due to vegetation restoration, conversion of areas with good moisture conditions to wetlands and poor moisture conditions to desert steppe. In the lower reaches of the HRB, the area of water bodies decreased in the 2000s due to the disappearance of the terminal lakes as a result of the disintegration of the Heihe River. However, the area of water bodies has increased as a result of the guaranteed downstream water supply since the implementation of the Heihe River Basin Plan in 2000. Although desert steppe is more vulnerable to precipitation variability, the area of desert steppe in the basin as a whole has

 doi:10.20944/preprints202406.0179.v1

continued to expand, particularly since 2010, with only minor decreases in the upper reaches in 2000 and in the lower reaches in 2010.

3.2. Pattern of Land Desertification Development and Reversal from 1990 to 2020

Usually, the increase or decrease in DL and NDL can be employed to describe the process of land desertification and restoration. However, it should be noted that degraded land accounts for a significant proportion of the HRB. Consequently, a more comprehensive understanding of the process of land desertification and restoration can be achieved by considering not only the changes between DL and NDL, but also the transformation of DL, NDL, and other land cover types. The transfer matrix of DL, NDL, and other land cover types in the period 1990-2000, 2000-2010, and 2010-2020 are shown in table 4, Table 5, and Table 6 respectively.

Table 4. Area of land desertification or land restoration in the HRB from 1990 to 2000 (km²).

	Cropland	Desert steppe	Water bodies	Artificial land	Sand	Wetland	Barren	NDL
				Upstream				
Cropland		1.29					0.08	1.23
Desert steppe	0.81		1.37	0.17		93.65	320.62	4144.96
Water bodies		1.26					0.47	2.68
Artificial land								
Wetland		8.34					17.25	193.82
Barren	0.74	3962.79	0.50	0.43		0.61		437.63
NDL	0.03	65.70	0.80	0.76		19.54	135.95	
				Midstream				
Cropland		53.05			0.03		19.51	12.77
Desert steppe	285.41		20.85	7.38	7.12	26.60	448.92	268.05
Water bodies		16.90			0.22		7.77	2.67
Artificial land								
Sand	7.32	29.88	3.33	0.06			31.37	0.23
Wetland		8.84			0.17		0.52	7.89
Barren	369.89	1488.42	22.94	36.32	3.23	0.89		39.28
NDL	76.75	67.53	1.23	0.73	0.04	4.04	2.67	
				Downstream				
Cropland		4.17					5.19	0.26
Desert steppe	4.61		1.41	0.02	14.59	0.02	235.58	47.96
Water bodies		1.43			0.10		66.31	0.02
Artificial land								
Sand		28.36	0.23				14.77	0.17
Wetland		0.58					0.06	0.63
Barren	2.92	633.94	1.64	4.96	0.97	0.04		0.85
NDL	1.47	36.94	0.04	0.04	0.05	0.01	0.83	
				Whole basin				
Cropland		58.50			0.03		24.78	14.26
Desert steppe	290.83		23.62	7.58	21.72	120.27	1005.12	4460.98
Water bodies		19.59			0.33		74.55	5.37
Artificial land								
Sand	7.32	58.24	3.56	0.06			46.14	0.40
Wetland		17.76			0.17		17.83	202.35
Barren	373.56	6085.15	25.07	41.72	4.21	1.54		477.77
NDL	78.25	170.16	2.07	1.52	0.09	23.59	139.45	

Table 5. Area of land desertification or land restoration in the HRB from 2000 to 2010 (km²).

 doi:10.20944/preprints202406.0179.v1

	Cropland	Desert steppe	Water bodies	Artificial land	Sand	Wetland	Barren	NDL
				Upstream				
Cropland		0.24						16.72
Desert steppe	2.85		2.03	2.19		10.80	381.44	1003.10
Water bodies		1.79					0.27	2.82
Artificial land								
Wetland		10.26					5.15	11.88
Barren	3.84	1573.00	0.31	0.45		19.48		130.95
NDL	0.98	419.30	1.70	1.43		307.54	413.93	
				Midstream				
Cropland		100.09					14.65	226.04
Desert steppe	344.20		6.45	9.31	1.48	21.21	229.86	460.13
Water bodies		30.09			0.42		7.29	4.09
Artificial land								
Sand	18.23	102.16	3.17	0.66			26.31	4.11
Wetland		2.69					0.06	3.93
Barren	615.16	2369.10	18.99	163.70	0.93	1.23		30.20
NDL	43.65	29.21	0.56	2.66		11.90	32.56	
				Downstream				
Cropland		2.92					0.51	3.79
Desert steppe	29.83		1.10	1.64	14.47	0.50	529.14	113.85
Water bodies		3.77			1.31		0.54	0.28
Artificial land								
Sand		56.70	0.94	0.14			29.38	0.26
Wetland		0.04						0.17
Barren	24.40	475.72	77.04	32.90	3.01	6.10		7.49
NDL	12.99	22.19	0.06	0.15	0.02		0.52	
				Whole basin				
Cropland		103.25					15.16	246.54
Desert steppe	376.87		9.57	13.15	15.96	32.51	1140.44	1577.08
Water bodies		35.65			1.73		8.09	7.18
Artificial land								
Sand	18.23	158.86	4.11	0.80			55.69	4.37
Wetland		12.99		0.15			5.21	15.98
Barren	643.41	4417.81	96.34	197.06	3.94	26.81		168.64
NDL	57.62	470.70	2.32	4.23	0.02	319.44	447.01	

Table 6. Area of land desertification or land restoration in the HRB from 2010 to 2020 (km^2).

	Cropland	Desert steppe	Water bodies	Artificial land	Sand	Wetland	Barren	NDL
				Upstream				
Cropland		0.49						9.34
Desert steppe	1.02		1.09	4.89		12.21	397.80	902.75
Water bodies		9.10					0.43	9.12
Artificial land								
Wetland		6.32					3.40	7.60
Barren		1374.68	0.39	0.39		5.70		373.50
NDL	1.46	703.13	1.75	3.82		41.26	37.27	
				Midstream				
Cropland		37.88					2.53	89.56
Desert steppe	328.79		12.91	42.90	4.27	17.47	118.81	862.46

 doi:10.20944/preprints202406.0179.v1

Water bodies		39.54			0.09		2.31	11.81
Artificial land								
Sand	44.14	233.25	0.75	7.53			12.04	2.47
Wetland		2.11					0.30	2.79
Barren	505.55	3990.09	23.78	344.22	8.52	2.59		70.47
NDL	50.27	77.14	2.30	1.69	0.01	20.36	9.17	
				Downstream				
Cropland		1.61					0.38	8.52
Desert steppe	4.79		5.21	2.22	6.07	4.80	50.28	280.51
Water bodies		7.30			0.07		1.12	2.36
Artificial land								
Sand		2493.67	4.75				1.98	0.48
Wetland		0.10					0.05	0.13
Barren	4.79	5536.33	15.05	25.49	2.72	4.34		48.02
NDL	5.20	11.97	0.30	0.23		0.81	0.11	
				Whole basin				
Cropland		39.98					2.91	107.42
Desert steppe	334.60		19.21	50.00	10.35	34.49	566.90	2045.72
Water bodies		55.95			0.16		3.87	23.29
Artificial land								
Sand	44.14	2726.92	5.50	7.53			14.03	2.95
Wetland		8.53					3.75	10.52
Barren	510.35	10901.10	39.22	370.10	11.23	12.63		491.99
NDL	56.93	792.24	4.35	5.74	0.01	62.43	46.55	

In this study, we define the conversion of DL to NDL, DL to Other, Other to NDL, and Sand or Barren to Desert steppe as land restoration processes, and the conversion of NDL to DL, Other to DL, NDL to Other, and Desert steppe to Sand or Barren as land desertification processes. Figure 3 shows the spatial distribution characteristics of land desertification and restoration between 1990 -2000, 2000-2010, and 2010-2020 in the HRB, and Figure 4 shows the statistical characteristics of the different land desertification or restoration processes in the different subregions of the HRB for each period.

 doi:10.20944/preprints202406.0179.v1

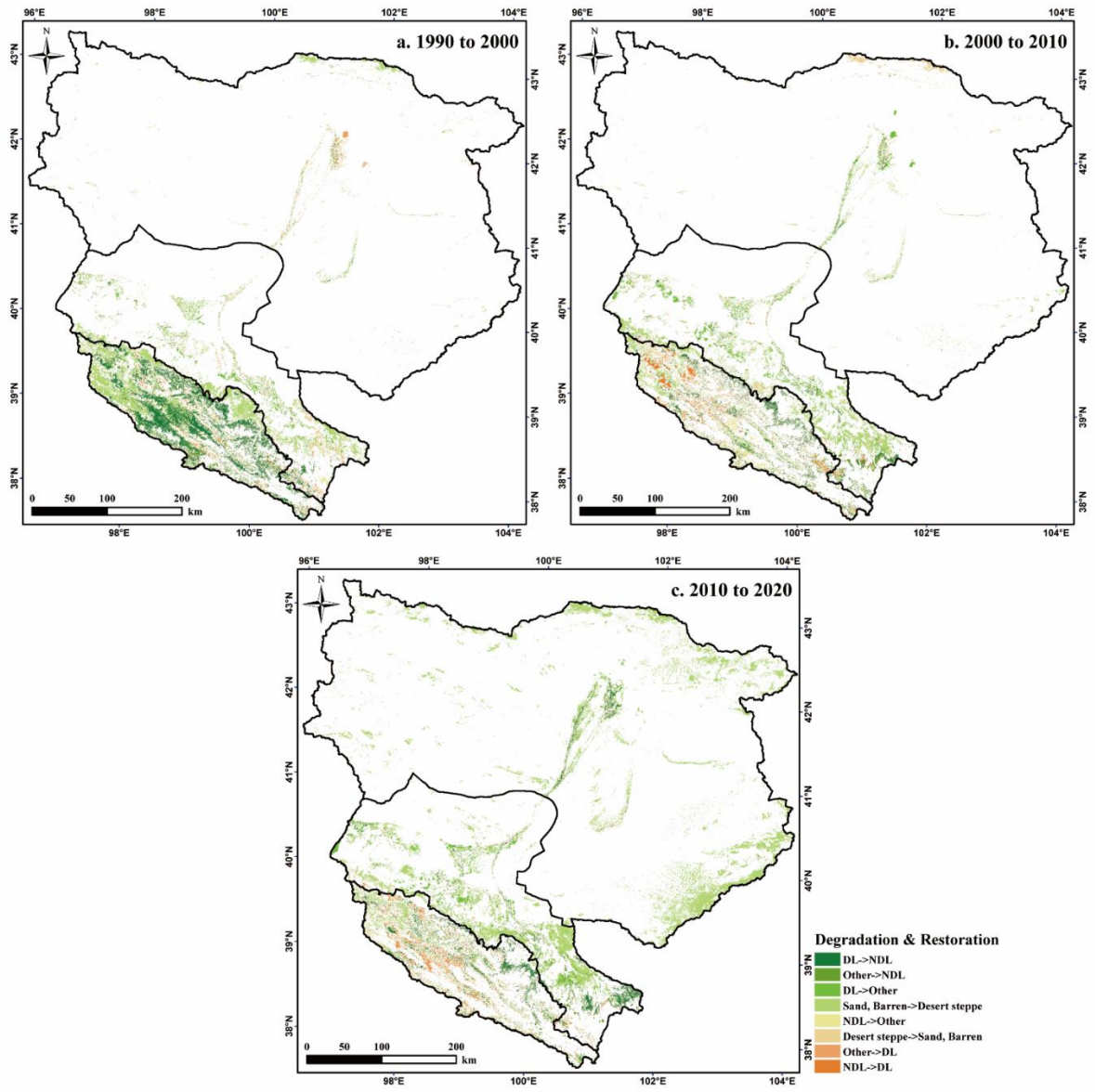

Figure 3. The pattern of land desertification and land restoration between 1990-2000, 2000-2010, and 2010-2020.

Preprints.org (www.preprints.org) | NOT PEER-REVIEWED | Posted: 4 June 2024 doi:10.20944/preprints202406.0179.v1

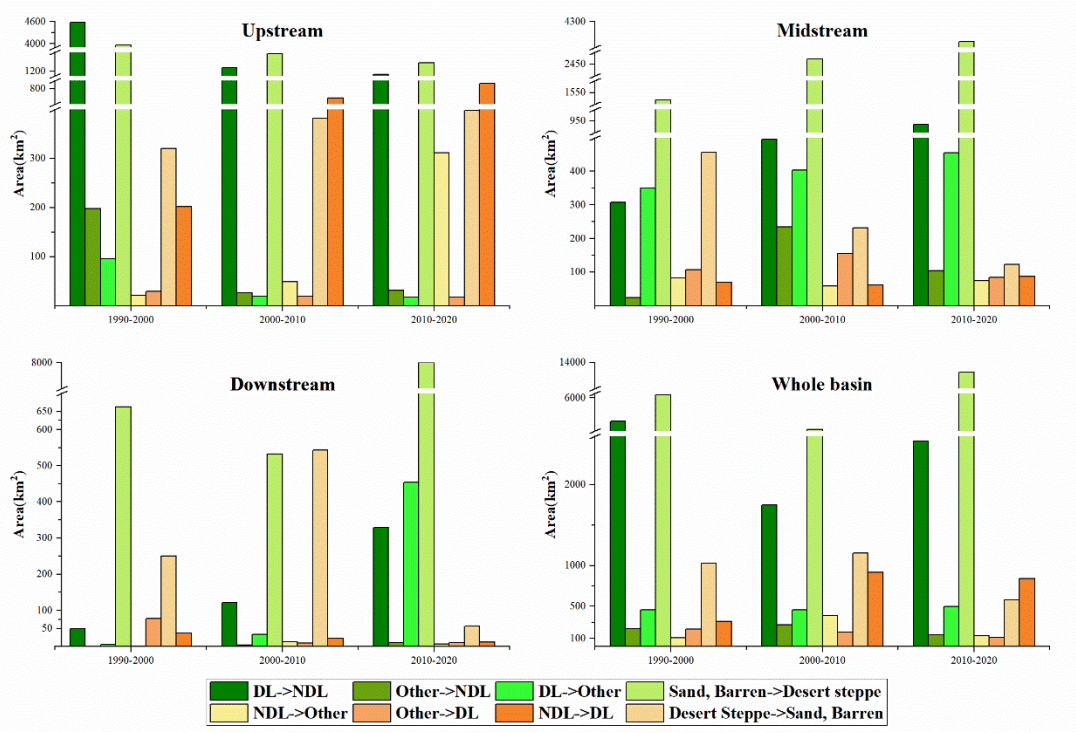

Figure 4. The trend of land desertification and land restoration process during the study period.

3.2.1. The Spatial Distribution Patterns of Land Desertification and Restoration in the HRB from 1990 to 2000

From 1990 to 2000, the area of HRB undergoing desertification is 1655.54 km², accounting for 0.61% of the total area. The main process of land desertification is the conversion of Desert steppe to Sand or Barren, which accounts for 62.02% of the degraded area, followed by the conversion of NDL to DL, Other to DL and NDL to Other, which account for 18.71%, 12.90% and 6.37% of the degraded area, respectively. The newly increased DL area is 523.26 km², accounting for 31.61% of the degraded area, of which 59.19% is degraded NDL. The reduced NDL area is 415.15 km², accounting for 25.08% of the degraded area, of which 74.60% is converted to DL. Regarding the various divisions of the HRB, land desertification is primarily concentrated in the midstream, which accounts for 43.25% of the total degraded area. This is followed by the upstream and downstream, which account for 34.56% and 22.19% of the degraded area, respectively. Although the process of land desertification in different subregions of the HRB is mainly Desert steppe to Sand or Barren, the upstream has a much larger proportion of NDL to DL than other regions, accounting for 35.25% of the degraded area, while the downstream has a minimal area of less than 1% of NDL to Other. Furthermore, the midstream has a relatively large area of NDL to Other. The newly increased DL in the upstream region is primarily derived from NDL, while the middle and downstream regions are mainly derived from Other. Conversely, the reduced NDL is primarily converted to Other in the middle reaches, and to DL in the upstream and downstream regions. Regarding the spatial distribution of land desertification, it can be observed that in the upstream, the phenomenon is concentrated in the flat areas of the broad valleys of the river. In the midstream, it is primarily located in the desert steppes in the south-east of Shandan County. Finally, in the downstream area, it is mainly observed on the banks of the river, within the oases, and in the terminal lakes and their surroundings.

From 1990 to 2000, the area of the HRB where land restoration is taking place was 11757.74 km², accounting for 4.34% of the total area. The main process of land restoration is the conversion of Sand or Barren to Desert Steppe, which accounts for 52.25% of the restored area, followed by the conversion of DL to NDL, DL to Other and Other to NDL, which account for 42.01%, 3.85% and 1.89% of the restored area respectively. The newly increased NDL area is 5161.11 km², accounting for 43.90% of the restored area, of which 95.70% was converted from DL. The reduced area of DL is 5392.38 km²,

 doi:10.20944/preprints202406.0179.v1

representing 45.86% of the restored area, of which 91.59% was converted to NDL. Regarding the different divisions of the HRB, land restoration is mainly concentrated in the upstream, which accounts for 75.18% of the total restored area. This is followed by mid-stream and downstream, which account for 18.71% and 6.11% of the restored area respectively. The main land restoration process in mid and low catchment, consistent with the whole catchment, is Sand or Barren to NDL. Especially in the downstream, more than 90% of the restoration was done in this way. For the upstream, the main land restoration process is conversion of DL to NDL and conversion of Sand or Barren to NDL, which account for 96.68% of the restored area, the former being slightly larger than the latter. The Midstream region differs from the other regions in that the conversion of DL to Other is relatively large and is the second major land restoration process, accounting for 15.95% of the restored area, in contrast to the Upstream and Downstream regions, which both account for about 1% of the restored area. A common feature of the different regions of the HRB is that the conversion of Other to NDL is small in all of them. In terms of the spatial distribution of land restoration, upstream land restoration occurs mainly in the floodplains and more arid western regions. Midstream land restoration is mainly concentrated around oases and desertified grasslands in the eastern parts. Land restoration in the downstream occurs mainly along the western and northern margins of the Badain Jaran desert, in addition to small patches in the northern parts of the region.

3.2.2. the spatial distribution patterns of land desertification and restoration in the HRB from 2000 to 2010

From 2000 to 2010, the area of the HRB undergoing is 2285.66km^2, accounting for 0.84% of total area. The rate of land desertification was slightly higher in this period than in the previous period. Although the main process of land desertification remains the conversion of Desert steppe to Sand or Barren, its proportion has decreased. Unlike in the previous period, the proportion of conversion of NDL to DL has increased considerably, accounting for 36.09% of the degraded area, while the proportion of the other two desertification processes has decreased. The newly increased DL area is 1009.02 km^2, and the reduced NDL area is 945.14 km^2, almost as twice as much as in the previous period, and the main sources of DL and destinations of NDL were the same as in the previous period, but with a greater weight. In terms of the different subregions of the HRB, land desertification occurs mainly in the upstream, accounting for 52.06% of the degraded area, followed by the downstream and midstream, which account for 25.75% and 22.19% of the degraded area, respectively. The main process of land desertification in the midstream and downstream is conversion of Desert steppe to Sand or Barren, consistent with the whole basin., especially in the downstream where it dominates with more than 90%. The main process of land desertification in the upstream is conversion of NDL to DL, accounts for 62.23% of the degraded area, followed by conversion of Desert steppe to Sand or Barren with a proportion of 32.06%. The newly increased DL in midstream is primarily derived from Other, while the upstream and downstream regions are mainly derived from NDL. Conversely, the reduced NDL is primarily converted to DL in different subregions, but the proportion of NDL converted to Other in the midstream in much larger than in the other regions. In terms of spatial distribution, land desertification in upstream is predominantly in the more arid regions of the northwest, while in the midstream and downstream it is predominantly sporadic in areas along rivers and adjacent to oases.

From 2000 to 2010, the area of land restored in the HRB was 7189.88km^2, representing 2.65% of the total area. The rate of land restoration in the HRB has slowed down, with only 61.14% of the area restored in the previous period. The conversion of Sand or Barren to Desert steppe remains the primary process of land restoration, although its proportion has increased. Furthermore, the proportion of conversion of DL to NDL is only half of what it was before, while the proportion of conversion of DL to Other has increased significantly. The newly increased NDL area is 2156.65 km^2, accounting for 30.00% of the restored area, of which 87.74% was converted from DL. The reduced area of DL is 2348.85 km^2, representing 32.67% of the restored area, of which 80.56% was converted to NDL. The decrease in area of newly increased NDL and in area of reduced of DL indicates a slowdown in the rate of land restoration in the HRB during this period. In terms of the different

 doi:10.20944/preprints202406.0179.v1

subregions of the HRB, land restoration during this period took place mainly in the midstream, which accounted for 50.11% of the entire restored area, followed by the upstream and downstream, which accounted for 40.26% and 9.63%, respectively. The main process of land restoration in all watershed subregions is the conversion of Sand or Barren to Desert steppe, with the conversion of DL to NDL as the second most important process of land restoration, especially in the upstream. In addition, the other two land restoration processes in the midstream accounted for a much larger proportion of land restoration than in the upstream and downstream. The main source of newly increased NDL in the different watershed subregions is from DL, but the proportion of Other converted to NDL is much larger in the midstream than in the other regions. Reduced DL converted primarily to NDL, especially in upstream, where this process of land restoration is absolutely dominant. The spatial distribution of land restoration in midstream and downstream is roughly the same as in the previous period, except that in the downstream there is a significant increase in land restoration along the banks of the river, in the oases and in the area of the terminated lakes.

3.2.3. The Spatial Distribution Patterns of Land Desertification and Restoration in the HRB from 2010 to 2020

From 2010 to 2020, the area of the HRB undergoing desertification is 2014.78 km^2, accounting for 0.74% of the total area. The rate of desertification was slower than in the period between 2000 and 2010, and comparable to the period between 1990 and 2000. In contrast to the previous two periods, the main process of land desertification is the conversion of NDL to DL between 2010 and 2020, which is accounted for 46.24% of total degraded area, followed by the conversion of Desert steppe to Sand or Barren, NDL to Other, and Other to DL, which accounting for 28.65%,19.50%, and 5.61%, respectively. The newly increased DL area is 1044.74km^2, accounting for 51.85% of degraded area, of which 89.17% is degraded NDL. The reduced NDL area is 1324.43 km^2, accounting for 65.74% of degrade area, of which 89.17% is converted to DL. Regarding the various divisions of the HRB, land desertification is primarily concentrated in the upstream, which accounts for 77.45% of the total degraded area, followed by midstream and downstream, which accounts for 20.23%, and 4.25% of the total degraded area, respectively. The main process of land desertification in the upstream is conversion of NDL to DL, and in midstream and downstream is the conversion of Desert steppe to Sand or Barren. The rate of desertification in midstream and downstream is not only significantly smaller than in the upstream, but also significantly smaller than in the other periods. The upstream accounts for the majority of both newly increased DL and reduction of NDL, suggesting that land desertification is more severe in the upstream. In terms of spatial distribution, land desertification is mainly concentrated in the pre-mountain plains and broad-valley steppe areas in the central and western regions of the upstream. Land desertification in the midstream is found in small patches in the south-eastern regions, and sporadically with in oases on a merit basis. Very few areas of land desertification in the downtown, mainly on the western edge of the desert and along the rivers.

From 2010 to 2020, the area of land restored in the HRB was 16667.17km^2, accounting for 6.15% of total area. The rate of land restoration has accelerated significantly during this period. The conversion of Sand or Barren to Desert steppe remains the primary process of land restoration, accounts for 81.77% of total restored area. The newly increased NDL area is 2545.03km^2, which is an increase in area over the previous period but a significant decrease in proportion, to only half of the previous period. The reduction area of DL is 2892.59 km^2, accounting for 17.35% of total restored area, of which 82.92% was converted into NDL. In terms of the different subregions of the HRB, land restoration occurs mainly in the downstream, which accounted for 50.35% of total restored area, followed by midstream and upstream, which accounted for 34.30%, 15.35% of total restored area, respectively. The conversion of Sand or Barren to Desert steppe remains the main process of land restoration in all watershed subregions. In addition, the conversion of DL to NDL is the second major land restoration process, especially in the upstream, accounting for 44.43% of total restored area. The main source of new NDL is from DL, and the reduced DL area mainly converted to NDL. It is only in the midstream that the proportion of conversion of DL to Other, and Other to NDL is much larger than in the other regions. In terms of spatial distribution, the areas where land restoration is occurring

 doi:10.20944/preprints202406.0179.v1

roughly the same as in the previous period, with an increase in the area restored. Furthermore, large area of restoration occurred in the north mountainous areas of the corridor in the north-eastern of midstream, and in downstream large areas of restoration occurred in the eastern desert region.

In summary, land desertification coexists with land restoration in the HRB. At different periods, the area of land restoration is much larger than the area of land desertification in the HRB (Figure 4), and the HRB has been in a process of land restoration. From Figure 4, it can be seen that the area of land restoration in the whole watershed decreases and then increases, while the area of land desertification increases and then decreases, indicating that land desertification is more serious from 2000 to 2010. It can also be seen that the area of land restoration in the upstream region continues to decrease and the area of desertification continues to increase, the area of land restoration in the middle region continues to increase and the area of desertification continues to decrease, and the area of land desertification in the downstream region continues to decrease, except for the area of Desert steppe converted to Sand or Barren, which is more sensitive to the effects of precipitation, which has increased from 2000 to 2010, suggesting that land desertification in the upstream region continues to worsen.

4. Discussion

Climate change and human activities were the two critical factors affecting land desertification or restoration processes, and could both influence land desertification on the regional scale (Dawelbait and Morari 2012). In this study, the driving factors of land desertification and restoration are revealed by analyzing changes in precipitation, temperature, population, cropland, livestock and politic measures.

4.1. Impact of Climate Change on Land Desertification

The HRB is a typical inland basin in the northwest of China, with a unique "Glacier permafrost-River-Oasis-Desert-Terminal lake" multifaceted natural landscape linked by water. The upper, middle and lower reaches of the HRB are three distinct geographical units. Therefore, we chose annual mean temperature, precipitation data recorded at Qilian, Zhangye and Ejina meteorological stations from 1975 to 2015 to characterize climate change in different subregions, respectively.

In the upstream of the HRB, both precipitation and mean annual temperatures show a significant upward trend, with a rate of change in mean annual temperature of 0.46℃/10a, which is 0.5 to 1 times the average warming of the Qing-Tibetan Plateau over the past four decades (Chen et al. 2015). Due to the high altitude, warmer temperatures help to alleviate the thermal constraints on vegetation growth, which promoted vegetation growth. Meanwhile, increased precipitation also contributed to vegetation growth. However, some scholars believe that increased temperatures is major climatic factor responsible for vegetation desertification in alpine regions (Song et al. 2020; Xue et al. 2009), as it causes the upper permafrost to thaw or disappear, and the disappearance of the impermeable layer formed by the presence of permafrost decreases the water content of the soil in the vegetation root zone, thus leading to changes in soil structure and composition, which is also the main reason for the desertification of alpine meadows and swampy meadows (Wang and Cheng 1999). In summary, taken together, the coexistence of land desertification and restoration processes is consistent with climate variability in the upstream of the HRB.

In the mid- and downstream, mean annual temperature also show a similarly significant upward trend, with warming rates greater than 0.5℃/10a. As the HRB is located in the northwestern arid zone of China, the increase in temperature has not been accompanied by a significant increase in precipitation, especially in the midstream, where precipitation has actually tended to decrease, which has led to an increase in the degree of aridity, further aggravating the water constraints on vegetation growth, both of which are unfavorable to the vegetation growth, leading to the development of land desertification. In addition, agricultural droughts caused by increased dryness will inevitably lead to a reduction in ecological water use as a result of enhanced irrigation to reduce water stress. As the cropland in the HRB is concentrated in midstream, the reduction in the amount of water released into

 doi:10.20944/preprints202406.0179.v1

the downstream as a result of heavy irrigation is a major factor contributing to downstream land desertification, especially between 1990 and 2000.

4.2. Impact of Human Activity on Land Desertification

The impact of human activities on desertification is twofold: on the one hand, irrational human activities such as overgrazing, over-cultivation and over-exploitation of water resources can exacerbate or accelerate the process of land desertification; on the other hand, rational human activities can slow down or even reverse desertification under adverse climatic conditions. In this study, we illustrate the impact of human activity on land desertification in five dimensions: population, the area of cropland, the number of livestock, politic measures and water resources.

The over-utilization of natural resources as a result of rapid population expansion is the root cause of all irrational human activities. Take Zhangye City as an example (Figure 6a), the population has increased from 68.25×10^4 in 1964 to 113.0×10^4 in 2020, with a particular peak in 2010(130.83×10^4), when the total number of people nearly doubled. A lager increase in population will inevitably lead to a significant increase in cropland, residential land, industrial land and land for transport. Which is the main reason for the significant decrease in DL since 2000. However, the lack of adequate protection of the land surface and the destruction of natural vegetation and soil structure due to the overexploitation of natural resources by population growth and irrational economic activities, coupled with strong wind erosion and the accumulation of surface soil salts caused by over-utilization of water resources are main factors contributing to land desertification.

Because the basin is landlocked, natural precipitation is not sufficient to support agricultural production, and therefore large amounts of water resources are needed for irrigation to meet the demands of agricultural production. With the increasing area of cropland and the adverse effects of climate warming, the irrigation demand in the midstream oasis has been increasing, and the downstream ecological water use has been drastically reduced (Figure 7), leading to serious ecological desertification downstream. In addition, when surface water resources are unable to meet irrigation, over-exploitation of groundwater to meet irrigation demand has caused the water table to fall, leading to the withering of natural vegetation around the oases. To cope with water shortages, the implementation of water-saving measures such as drip pipes and furrow lining has reduced irrigation used to some extent, but has also reduced the amount of water that infiltrates, which has resulted in a lack of water recharge for the natural vegetation in oases, and numerous drying out of the vegetation, leading to land desertification.

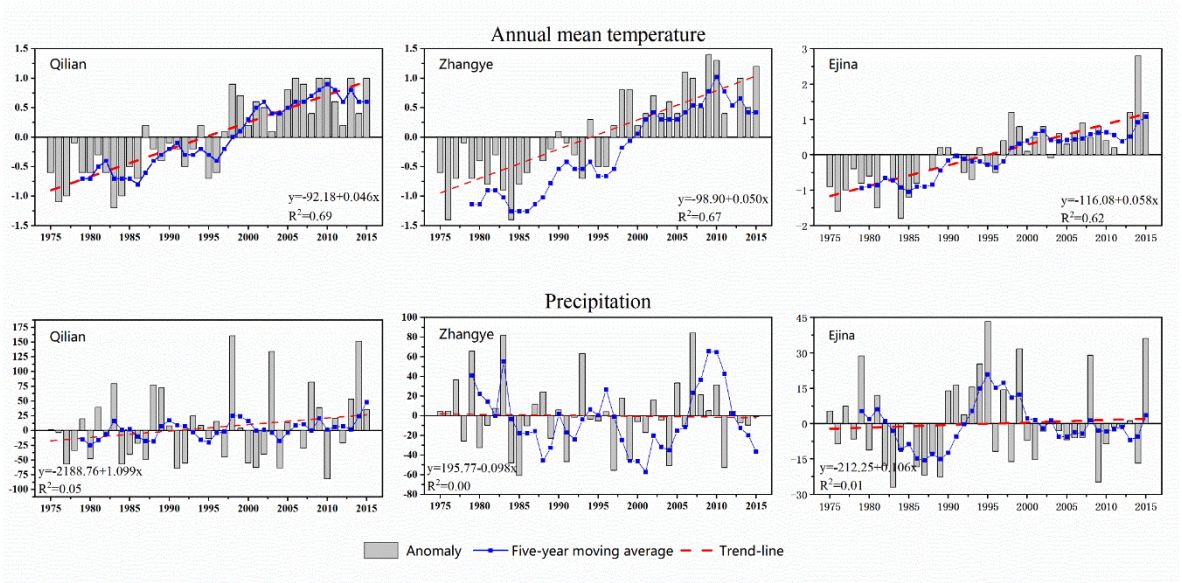

Figure 5. Change in annual mean temperature, precipitation in the Heihe River Basin from 1975 to 2015.

 doi:10.20944/preprints202406.0179.v1

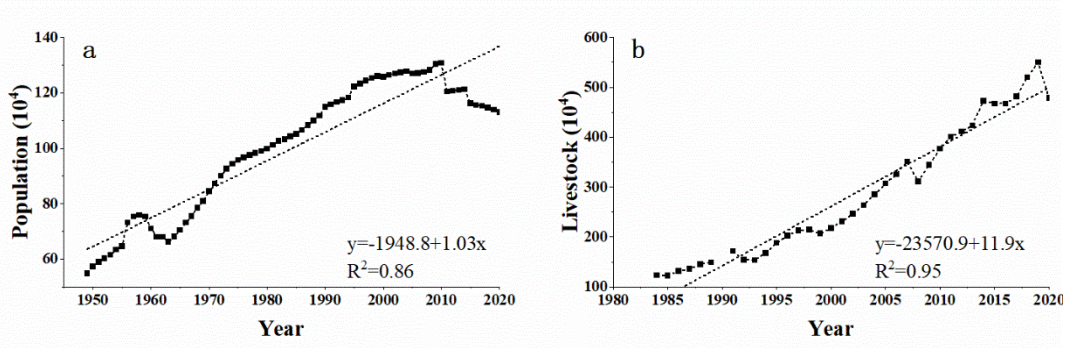

Figure 6. Change in population and livestock in Zhangye City.

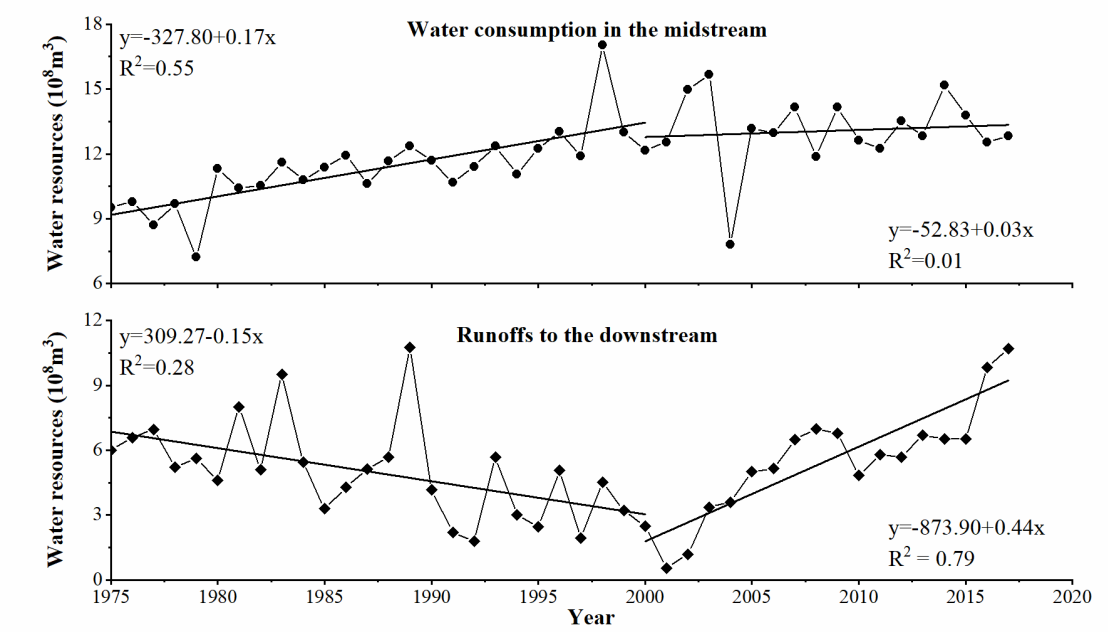

Figure 7. Change in water consumption in the midstream and runoffs to the downstream from 1975 to 2017.

Overgrazing is another major cause of land desertification in the HRB. The population of livestock has been increasing linearly since the 1980s. Taking sheep farming in Zhangye City as an example (Figure 6b), the sheep population in 2020 was 446.6% of that in 1984. Rapidly increasing livestock numbers are making overgrazing widespread in the HRB. Furthermore, over-exploitation of valuable medicinal plants such as *Ephedra*, *Cistanche*, *Cordyceps*, *Licorice*, etc. is also a major factor in desertification of natural grassland.

To curb land desertification and protect the ecological environment, the Chinese government has implemented a series of ecological protection and restoration measures, such as the "Three-North Shelterbelt Project", "Grain for Green", "the Natural Forest Protection Project", "Grazing Withdrawal Program", "Construction of Nation Ecological Security Barriers". In the HRB, the exclusion of grazing in degraded grassland, closed breeding, rehabilitation and use of saline land, Ecological Water Diversion Project(EWDP) have been adopted to combat land desertification and rehabilitate the degraded environment. In addition, as one of the main bases for the development and construction of new energy sources in China, the construction of ecological PV power plants using the "PV + sand control" model has also significantly reduced desertified land in the HRB. These measures and policies play an important role in controlling desertification and restoring vegetation.

 doi:10.20944/preprints202406.0179.v1

5. Conclusions

In this study, 30m high-resolution information on land desertification and restoration in the HRB was extracted using remote sensing interpretation and GIS spatial analysis methods. Our results show that land desertification coexists with land restoration in the HRB. At different periods, the area of land restoration is much larger than the area of land desertification in the HRB, and the HRB has been in a process of land restoration. In upstream of the HRB, there is a continuing trend of increasing land desertification and a continuing slowdown in land restoration. In the middle and downstream, desertification continues to decrease, while land restoration continues to increase. Increasing desertification upstream is associated with overgrazing in a context where climate change favors desertification reversal. Although both climate variability and human activities favor land desertification, the process of land desertification in the middle and lower reaches is still being reversed and land restoration dominates. The implementation of the eco-environmental protection project and desertification control measures, particularly the EWDP, is contributing to the reversal of desertification in the middle and lower reaches of the HRB. However, the EWDP is indirectly contributing to the lowering of the water table in the middle reaches through the expansion of cropland and the implementation of water-saving irrigation systems. There is therefore an urgent need to transform the economic structure of the middle reaches, which is dominated by water-intensive agriculture, to cope with water scarcity and land desertification.

Acknowledgments: This study is supported by Nation Key Research and Development Program (Grant No.2020YFA0608401), the National Natural Science Foundation of China (Grant No.41801072), the Second Tibetan-Plateau Scientific Expedition and Research Program (STEP, Grant No.2019QZKK0305), and the Open Fund Project of the Key Laboratory of Desert and Desertification, Chinese Academy of Sciences (KLDD-2018-001).

References

1. Amani, M., Ghorbanian, A., Ahmadi, S.A., Kakooei, M., Moghimi, A., Mirmazloumi, S.M., Moghaddam, S.H.A., Mahdavi, S., Ghahremanloo, M., & Parsian, S. (2020). Google earth engine cloud computing platform for remote sensing big data applications: A comprehensive review. IEEE Journal of Selected Topics in Applied Earth Observations and Remote Sensing, 13, 5326-5350
2. Burrell, A.L., Evans, J.P., & Liu, Y. (2018). The impact of dataset selection on land degradation assessment. ISPRS Journal of Photogrammetry and Remote Sensing, 146, 22-37
3. Chen, D., Xu, B., Yao, T., Guo, Z., Cui, P., Chen, F., Zhang, R., Zhang, X., Zhang, Y., & Fan, J. (2015). Assessment of past, present and future environmental changes on the Tibetan Plateau. Chin. Sci. Bull, 60, 3025-3035
4. Chen, T.K., Qiu, C., Schmitt, M., Zhu, X.X., Sabel, C.E., & Prishchepov, A.V. (2020). Mapping horizontal and vertical urban densification in Denmark with Landsat time-series from 1985 to 2018: A semantic segmentation solution. Remote Sensing of Environment, 251, 112096
5. Christian, B.A., & Dhinwa, P. (2018). Long term monitoring and assessment of desertification processes using medium & high resolution satellite data. Applied Geography, 97, 10-24
6. Ci, L. (2000). Understanding on the term of "desertification". Chinese Science and Technology Terms Journal, 2, 11-13
7. Dawelbait, M., & Morari, F. (2012). Monitoring desertification in a Savannah region in Sudan using Landsat images and spectral mixture analysis. Journal of Arid Environments, 80, 45-55
8. Duan, H., Wang, T., Xue, X., & Yan, C. (2019). Dynamic monitoring of aeolian desertification based on multiple indicators in Horqin Sandy Land, China. Science of The Total Environment, 650, 2374-2388
9. Dwyer, J., Roy, D., Sauer, B., Jenkerson, C., Zhang, H., & Lymburner, L. (2018). Analysis ready data: enabling analysis of the Landsat archive. Remote Sens. 10, 1363. In
10. Gichenje, H., & Godinho, S. (2018). Establishing a land degradation neutrality national baseline through trend analysis of GIMMS NDVI Time-series. Land Degradation & Development, 29, 2985-2997
11. Guo, B., Wei, C., Yu, Y., Liu, Y., Li, J., Meng, C., & Cai, Y. (2022). The dominant influencing factors of desertification changes in the source region of Yellow River: Climate change or human activity? Science of The Total Environment, 813, 152512
12. Guo, B., Zang, W., Han, B., Yang, F., Luo, W., He, T., Fan, Y., Yang, X., & Chen, S. (2020). Dynamic monitoring of desertification in Naiman Banner based on feature space models with typical surface parameters derived from LANDSAT images. Land Degradation & Development, 31, 1573-1592

 doi:10.20944/preprints202406.0179.v1

13. Hird, J.N., DeLancey, E.R., McDermid, G.J., & Kariyeva, J. (2017). Google Earth Engine, open-access satellite data, and machine learning in support of large-area probabilistic wetland mapping. Remote Sensing, 9, 1315
14. Huang, J., Yu, H., Guan, X., Wang, G., & Guo, R. (2016). Accelerated dryland expansion under climate change. Nature Climate Change, 6, 166-171
15. Koutroulis, A.G. (2019). Dryland changes under different levels of global warming. Science of The Total Environment, 655, 482-511
16. Lamchin, M., Lee, J.-Y., Lee, W.-K., Lee, E.J., Kim, M., Lim, C.-H., Choi, H.-A., & Kim, S.-R. (2016). Assessment of land cover change and desertification using remote sensing technology in a local region of Mongolia. Advances in Space Research, 57, 64-77
17. Lee, B.X., Kjaerulf, F., Turner, S., Cohen, L., Donnelly, P.D., Muggah, R., Davis, R., Realini, A., Kieselbach, B., & MacGregor, L.S. (2016). Transforming our world: implementing the 2030 agenda through sustainable development goal indicators. Journal of public health policy, 37, 13-31
18. Li, Q., Zhang, C., Shen, Y., Jia, W., & Li, J. (2016). Quantitative assessment of the relative roles of climate change and human activities in desertification processes on the Qinghai-Tibet Plateau based on net primary productivity. Catena, 147, 789-796
19. Li, S., He, S., Xu, Z., Liu, Y., & von Bloh, W. (2023). Desertification process and its effects on vegetation carbon sources and sinks vary under different aridity stress in Central Asia during 1990–2020. Catena, 221, 106767
20. Liu, Q., Liu, G., & Huang, C. (2018). Monitoring desertification processes in Mongolian Plateau using MODIS tasseled cap transformation and TGSI time series. Journal of Arid Land, 10, 12-26
21. Ma, X., Zhu, J., Yan, W., & Zhao, C. (2021). Projections of desertification trends in Central Asia under global warming scenarios. Science of The Total Environment, 781, 146777
22. Mariano, D.A., dos Santos, C.A., Wardlow, B.D., Anderson, M.C., Schiltmeyer, A.V., Tadesse, T., & Svoboda, M.D. (2018). Use of remote sensing indicators to assess effects of drought and human-induced land degradation on ecosystem health in Northeastern Brazil. Remote Sensing of Environment, 213, 129-143
23. Meng, X., Gao, X., Li, S., Li, S., & Lei, J. (2021). Monitoring desertification in Mongolia based on Landsat images and Google Earth Engine from 1990 to 2020. Ecological Indicators, 129, 107908
24. Nations, U. (2016). Transforming our world: The 2030 agenda for sustainable development
25. Shen, X., An, R., Feng, L., Ye, N., Zhu, L., & Li, M. (2018). Vegetation changes in the three-river headwaters region of the tibetan plateau of china. Ecological Indicators, 93, 804-812
26. Shi, Y., Shen, Y., Li, D., Zhang, G., Ding, Y., Hu, R., & Kang, E. (2003). Discussion on the present climate change from warm-dry to warm wet in northwest China. Quaternary Sciences, 23, 152-164
27. Song, X., Liao, J., Xue, X., & Ran, Y. (2020). Multi-Sensor Evaluating Effects of an Ecological Water Diversion Project on Land Degradation in the Heihe River Basin, China. Frontiers in Environmental Science, 8, 1-17
28. Song, X., Wang, T., Xue, X., Yan, C., & Li, S. (2015). Monitoring and analysis of aeolian desertification dynamics from 1975 to 2010 in the Heihe River Basin, northwestern China. Environmental Earth Sciences, 74, 3123-3133
29. Song, X., & Yan, C. (2014). Land cover change detection using segment similarity of spectrum vector based on knowledge base. Acta Ecol. Sinica, 34, 7175-7180
30. Tavares, J.D.P., Baptista, I., Ferreira, A.J., Amiotte-Suchet, P., Coelho, C., Gomes, S., Amoros, R., Dos Reis, E.A., Mendes, A.F., & Costa, L. (2015). Assessment and mapping the sensitive areas to desertification in an insular Sahelian mountain region Case study of the Ribeira Seca Watershed, Santiago Island, Cabo Verde. Catena, 128, 214-223
31. UNCCD (1999). United Nations Convention to Combat Desertification in Those Countries Experiencing Serious Drought And/or Desertification, Particulary in Africa. In: Secretariat of the United Nations Convention to Combat Desertification
32. Wang, G., & Cheng, G. (1998). Changes of hydrology and ecological environment during late 50 years in Heihe River Basin. J Desert Res, 18, 233-238
33. Wang, G., & Cheng, G. (1999). The ecological features and significance of hydrology within arid inland river basins of China. Environmental Geology, 37, 218-222
34. Wei, H., Wang, J., & Han, B. (2020). Desertification information extraction along the China–Mongolia railway supported by multisource feature space and geographical zoning modeling. IEEE Journal of Selected Topics in Applied Earth Observations and Remote Sensing, 13, 392-402
35. Wessels, K.J., Van Den Bergh, F., & Scholes, R. (2012). Limits to detectability of land degradation by trend analysis of vegetation index data. Remote Sensing of Environment, 125, 10-22
36. Wu, B., Yuan, Q., Yan, c., Wang, Z., Yu, X., Li, A., Ma, R., Huang, J., Chen, J., & Chang, C. (2014). Land cover changes of China from 2000 to 2010. Quaternary Sciences, 34, 723-731
37. Wu, Z., Lei, S., Bian, Z., Huang, J., & Zhang, Y. (2019). Study of the desertification index based on the albedo-MSAVI feature space for semi-arid steppe region. Environmental Earth Sciences, 78, 1-13

 doi:10.20944/preprints202406.0179.v1

38. Wulder, M.A., White, J.C., Loveland, T.R., Woodcock, C.E., Belward, A.S., Cohen, W.B., Fosnight, E.A., Shaw, J., Masek, J.G., & Roy, D.P. (2016). The global Landsat archive: Status, consolidation, and direction. Remote Sensing of Environment, 185, 271-283
39. Xu, D., Song, A., Tong, H., Ren, H., Hu, Y., & Shao, Q. (2016). A spatial system dynamic model for regional desertification simulation–A case study of Ordos, China. Environmental Modelling & Software, 83, 179-192
40. Xue, X., Guo, J., Han, B., Sun, Q., & Liu, L. (2009). The effect of climate warming and permafrost thaw on desertification in the Qinghai–Tibetan Plateau. Geomorphology, 108, 182-190
41. Yan, F., Wu, B., & Wang, Y. (2015). Estimating spatiotemporal patterns of aboveground biomass using Landsat TM and MODIS images in the Mu Us Sandy Land, China. Agricultural and Forest Meteorology, 200, 119-128
42. Zan, G., Wang, C., Li, F., Liu, Z., & Sun, T. (2023). Key Data Results and Trend Analysis of the Sixth National Survey on Desertification and Sandification. For. Resour. Manag, 1-7
43. Zhang, A., Zheng, C., Wang, S., & Yao, Y. (2015). Analysis of streamflow variations in the Heihe River Basin, northwest China: Trends, abrupt changes, driving factors and ecological influences. Journal of Hydrology: Regional Studies, 3, 106-124
44. Zhang, C., Li, Q., Shen, Y., Zhou, N., Wang, X., Li, J., & Jia, W. (2018). Monitoring of aeolian desertification on the Qinghai-Tibet Plateau from the 1970s to 2015 using Landsat images. Science of The Total Environment, 619, 1648-1659
45. Zhang, L., Wu, B., Li, X., & Xing, Q. (2014). Classification system of China land cover for carbon budget. Acta Ecologica Sinica, 34, 7158-7166
46. Zhang, Z., & Huisingh, D. (2018). Combating desertification in China: Monitoring, control, management and revegetation. Journal of Cleaner Production, 182, 765-775
47. Zhao, Y., Chang, C., Zhou, X., Zhang, G., & Wang, J. (2024). Land use significantly improved grassland degradation and desertification states in China over the last two decades. Journal of Environmental Management, 349, 119419
48. Zhou, Y., Dong, J., Xiao, X., Liu, R., Zou, Z., Zhao, G., & Ge, Q. (2019). Continuous monitoring of lake dynamics on the Mongolian Plateau using all available Landsat imagery and Google Earth Engine. Science of The Total Environment, 689, 366-380
49. Zhu, Z., Wang, S., & Woodcock, C.E. (2015). Improvement and expansion of the Fmask algorithm: Cloud, cloud shadow, and snow detection for Landsats 4–7, 8, and Sentinel 2 images. Remote Sensing of Environment, 159, 269-277
50. Zhu, Z., & Woodcock, C.E. (2014). Automated cloud, cloud shadow, and snow detection in multitemporal Landsat data: An algorithm designed specifically for monitoring land cover change. Remote Sensing of Environment, 152, 217-234
51. UNCCD, 2017. The Global Land Outlook. 1st ed. United Nations Convention to Combat Desertification, Bonn, Germany.
52. IPBES, 2018. In: Montanarella, L., Scholes, R., Brainich, A. (Eds.), The IPBES Assessment Report on Land Degradation and Restoration. Secretariat of the Intergovernmental Science-Policy Platform on Biodiversity and Ecosystem Services, Bonn, Germany Retrieved from. https://www.ipbes.net/.
53. Zhang, Q., C. J. Zhang, H. Z. Bai, et al., 2010: New development of climate change in Northwest China and its impact on arid environment. J. Arid Meteor., 28, 1–7